Histol Histopathol (2024) 39: 249-258

Histology and Histopathology
From Cell Biology to Tissue Engineering

ORIGINAL ARTICLE Open Access

Aromadendrin alleviates LPS-induced kidney apoptosis and inflammation by inhibiting phosphorylation of MAPK and NF-κB signaling pathways

Xiaohong Ma[1], Wenhua Liu[2], Bin Wang[2] and Feizhuang Shi[2]

[1]Department of Nephrology and [2]Department of Internal Medicine, Shenzhen Bao'an Authentic TCM Therapy Hospital, Shenzhen, China

Summary. Background. Excessive inflammation and apoptosis in kidneys are critical players in the pathogenesis of acute kidney injury (AKI). Aromadendrin is a natural flavonoid characterized by anti-inflammatory, anti-apoptotic, and antioxidant actions. Thus, we investigated the roles and mechanisms of aromadendrin in the development of AKI.

Methods. Lipopolysaccharide (LPS) was used to induce AKI mice, and one hour after LPS challenge, the mice received oral administration of aromadendrin or vehicle. Renal functions were assessed by measuring blood urea nitrogen and creatinine in serum. Histological changes were determined by hematoxylin and eosin staining. Apoptotic cells of renal tissues were detected by TUNEL staining. Gene expression was measured by western blotting and RT-qPCR.

Results. Aromadendrin alleviated LPS-induced renal dysfunctions and histological defects in mice. Additionally, aromadendrin suppressed excessive inflammation and tissue apoptosis in the kidneys of LPS-induced AKI mice. Mechanistically, aromadendrin blocked the activation of NF-κB and MAPK pathways in LPS-induced AKI mice.

Conclusion. Aromadendrin alleviates LPS-stimulated inflammation and tissue cell apoptosis in kidneys by inactivating the NF-κB and MAPK pathways.

Key words: Acute kidney injury, Aromadendrin, Apoptosis, Inflammatory response, LPS, NF-κB, MAPK

Introduction

Acute kidney injury (AKI) represents a syndrome with clinical characteristics such as decreased glomerular filtration rate (GFR), increased blood urea nitrogen (BUN) and serum creatinine, and oliguria. Major complications of AKI include hyperkalemia, volume overload, metabolic acidosis, and hypernatremia (Ichai et al., 2016). As estimated, 2-5% of patients develop AKI during hospitalization, and the incidence rises to 67% among patients admitted to the ICU (Goyal et al., 2023). In an analysis of 47,017 in-hospital patients, the mortality rate of AKI reaches 8.9% (Coca et al., 2009). AKI is amenable to prevention, early detection, and treatment. The current standard methods for AKI management include hemodynamic management, a combination of nephrotoxin stewardship and novel biomarkers, and renal replacement therapy (Yoon et al., 2022). These methods improve the clinical outcomes of AKI; however, the incidence and mortality of SKI are still high. Therefore, a better understanding of the underlying mechanisms of AKI and the search for novel effective therapeutic options are urgent.

Podocytes are terminally differentiated epithelial cells attached to the outside of the glomerular basement membrane (GBM) in the kidney (Reiser and Altintas, 2016). Podocyte injury contributes to proteinuria and ultimately renal dysfunction through podocyte cytoskeleton disorder and foot process fusion (Sever and Schiffer, 2018). Compelling evidence has suggested that podocyte apoptosis is regarded as an essential contributor to the development of glomerular disease and is associated with progressive AKI (Gong et al., 2022; Ma et al., 2022; Zhang et al., 2023). In addition to podocyte injury, excessive inflammation is a critical player in the pathogenesis of AKI. Tubular epithelial cell damage leads to activation of resident immune cells, initiating the inflammatory response in the kidney (Basile et al., 2012; Dellepiane et al., 2016; Guzzi et al., 2019). Endotoxin lipopolysaccharides (LPS) are derived from the outer membrane of gram-negative bacterial cell

Corresponding Author: Xiaohong Ma, Shenzhen Bao'an Authentic TCM Therapy Hospital, No.99 Lai'an Road, Xixiang Street, Bao'an District, Shenzhen, Guangdong, PR China. e-mail: maxhdoctor@hotmail.com
www.hh.um.es. DOI: 10.14670/HH-18-770

walls and can induce the pathogenesis of inflammation-associated diseases (Van Amersfoort et al., 2003; Ding et al., 2018). Currently, LPS is widely used to induce AKI-like conditions (Chen et al., 2018; Zhang et al., 2021). LPS can bind to TLR4, activating NF-κB and MAPKs and increasing transcription of proinflammatory cytokines (Yoo et al., 2014; Zhuo et al., 2019). Excessive inflammation can promote tubular cell apoptosis and affect renal parenchyma, thereby inducing AKI occurrence (Dellepiane et al., 2016; Peerapornratana et al., 2019). Thus, the regulation of podocyte injury and kidney inflammation may be helpful in the treatment of AKI.

Aromadendrin is a flavonol widely found in *Chionanthus retusus*, *Pinus sibirica*, and *Afzelia bella*. Its antitumor, anti-inflammatory, anti-diabetic, and radical scavenging activities have been well established (Zhang et al., 2006, 2011; Lee et al., 2009). Aromadendrin can stimulate glucose uptake and attenuate insulin resistance to exert anti-diabetic effects (Zhang et al., 2011). Aromadendrin has also been found to exert its pharmacological activity by blocking the NF-κB and MAPK pathways (Lee and Jeong, 2020; Lee et al., 2013). However, the roles of aromadendrin in LPS-stimulated kidney apoptosis and inflammation in AKI remain uncertain.

In the current study, we investigated the roles and mechanisms of aromadendrin in LPS-induced AKI. We speculated that aromadendrin might alleviate LPS-induced AKI by inhibiting apoptosis and inflammation. Our study provides a novel pharmacological agent that could suppress kidney apoptosis and inflammation caused by LPS.

Materials and methods

Animals

C57BL/6 mice (male, 6-8 weeks of age) obtained from Charles River Laboratories (Beijing, China) were housed under standard conditions (25±2°C, 50% humidity, 12h light/dark cycle). Normal chow and water were provided *ad libitum*. All experimental protocols and procedures complied with the National Institutes of Health Guide for the Care and Use of Laboratory Animals and were approved by the Ethics Review Committee of Wuhan Myhalic Biotechnology Co., Ltd (HLK-202206126).

Experimental protocol

After 2 weeks of acclimation, the mice were randomly divided into the control group (n=18), the aromadendrin group (10 mg/kg) (n=18), the LPS (10 mg/kg) group (n=18), the LPS (10 mg/kg) + DMSO group (n=18), and the LPS (10 mg/kg) + Aromadendrin (10 mg/kg) group (n=18). To induce AKI-like conditions *in vivo*, the mice received LPS (10 mg/kg in 0.9% saline; MedChemExpress, Shanghai, China) via intraperitoneal injection. The dose of LPS was determined according to previous publications (Tang et al., 2021; Ban et al., 2022). One hour after LPS challenge, the mice were given 10 mg/kg aromadendrin (InvivoChem, Guangzhou, China) dissolved in 1% DMSO (Solarbio, Beijing, China) or the same volume of 1% DMSO via oral administration every 6h until sacrifice. To evaluate aromadendrin cytotoxicity, normal mice were administered 10 mg/kg dissolved in DMSO orally every 6h until sacrifice. The dose of aromadendrin was chosen as previously documented (Park et al., 2023). At 12, 24, and 48h after LPS challenge, the mice were sacrificed under pentobarbital anesthesia, and blood and kidney tissue samples were collected for further study.

Measurement of BUN and creatinine activities

After the mice were sacrificed at the indicated time, the thoracic cavity was cut, and blood samples were taken by heart puncture and maintained in anti-coagulation tubes. After being solidified, the serum was collected by centrifugation (5000 rpm, 15 min). The serum levels of mouse BUN, creatinine, and LDH were detected via the urease method using the BUN detection kit (Jiancheng Bioengineering Institute, Nanjing, China), the creatine oxidase method using the creatinine detection kit (Jiancheng), and the colorimetric method using the LDH assay kit (Jiancheneg). Each sample was tested three times and the average value was taken.

Histopathological analysis

After the collection of blood samples, renal arteries and veins were ligated using vascular clamps, and the two kidneys were collected with excess fat being removed. Unilateral kidney samples were fixed in 4% paraformaldehyde overnight at 4°C, dehydrated, embedded in paraffin, and cut into 5-μm slices. Then, the sections were deparaffinized using xylene, hydrated, and stained with hematoxylin-eosin (H&E; Solarbio, Beijing, China). Hematoxylin was added, and the samples were incubated at room temperature for 5 min. After being washed, eosin was added, and the samples were incubated at room temperature for 2 min. A light microscope (Olympus, Tokyo, Japan) was used to capture the images. The glomerular and tubular damage were scored semi-quantitatively using the following scoring system by two independent pathologists (Kökény et al., 2017; Liang et al., 2017). Glomerular damage: grade 0, no change, healthy glomerulus; grade 1, lining of capillaries to Bowman's capsule; grade 2, accumulation of mesangial matrix in 25% of the glomerulus; grade 3, accumulation of mesangial matrix in 50% of the glomerulus and capillary obliteration; and grade 4, accumulation of mesangial matrix in 75% of the glomerulus. Tubular damage was scored based on the percentage of damaged tubules: grade 0, no damage; grade 1, minimal damage (<25%

damage); grade 2, mild damage (25-50% damage); grade 3, moderate damage (50-75% damage); and grade 4, severe damage (>75% damage). The glomerular and tubular scores of each animal were derived as the arithmetic mean of 60-80 glomeruli or 15-20 observation fields, respectively.

RT-qPCR

Total RNA was isolated from kidney tissues using TRIzol reagent (Beyotime) and quantified by NanoDrop spectrophotometry (Thermo Fisher Scientific). The reverse transcription of RNA into cDNA was performed using the BeyoRT™ first-strand cDNA synthesis kit (Beyotime). Then, cDNA was amplified by RT-qPCR in a reaction containing SYBR Green PCR Master Mix (Solarbio) and 0.2 μm primers and analyzed using the ABI 7500 Fast Real-Time PCR system (Thermo Fisher Scientific). The amplification level was programmed with a denaturation step of 3 min at 95°C, followed by 40 cycles of denaturation at 95°C for 12 s, and extension at 62°C for 40 s. Data were normalized to GAPDH and expressed as fold changes over control. The $2^{-\Delta\Delta Ct}$ method was used to determine the relative mRNA fold changes (Livak and Schmittgen, 2001). The primers used in this study are listed in Table 1.

Western blotting

Total protein was isolated from kidney tissues using RIPA lysis buffer (Sigma-Aldrich) containing 1% protease inhibitor (Beyotime), and the protein content was quantified with an Enhanced BCA Protein assay kit (Beyotime). Then, protein samples (30 μg/group) were separated by 12% sodium dodecyl sulfate-polyacrylamide gel electrophoresis (SDS-PAGE) gel and

Table 1. Sequences of primers used for reverse transcription-quantitative PCR.

Gene (mice)	Sequence (5'✳3')
TNF-α forward	CCAGACCCTCACACTCACAAA
TNF-α reverse	GGCTGACGGTGTGGGTGAG
IL-1β forward	TCCTGTGTAATGAAAGACGGC
IL-1β reverse	TGCTTGTGAGGTGCTGATGTA
IL-6 forward	ATGGCAATTCTGATTGTATG
IL-6 reverse	GACTCTGGCTTTGTCTTTCT
MCP-1 forward	CTTCT GGGCCTGCTGTTCA
MCP-1 reverse	CCAGCCTACTCATT GGGATCA
GAPDH forward	GAGCCAAAAGGGTCATCATC
GAPDH reverse	TAAGCAGTTGGTGGTGCAGG

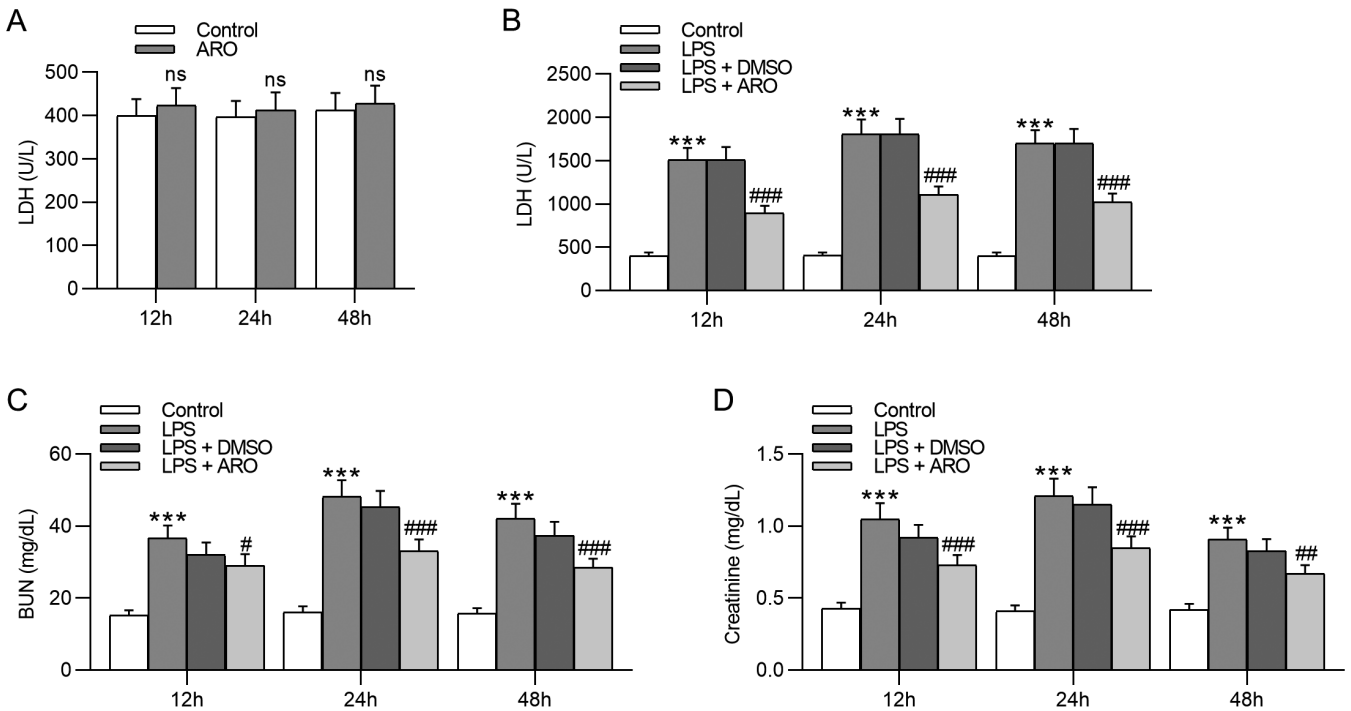

Fig. 1. Aromadendrin alleviates LPS-induced renal dysfunctions in mice. **A.** Serum LDH levels in the control and aromadendrin groups at 12, 24, and 48h after aromadendrin administration. **B.** Serum LDH levels in the control, LPS, LPS + DMSO, and LPS + aromadendrin groups at 12, 24, and 48h after LPS challenge. **C.** Serum BUN levels in different groups at the indicated time points. **D.** Serum creatinine levels in different groups at the indicated time points. Data are expressed as mean ± standard deviation. n=6 mice per group. ns, not significant; ***p<0.001 vs. Control group; $^{\#}p$<0.05, $^{\#\#}p$<0.01, $^{\#\#\#}p$<0.001 vs. LPS group. LPS, lipopolysaccharide; DMSO, dimethyl sulfoxide; LDH, lactate dehydrogenase; BUN, blood urea nitrogen.

transferred onto polyvinylidene fluoride (PVDF) membranes. After being blocked using 5% skimmed milk at room temperature for 2h, the membranes were incubated overnight with primary antibodies against COX-2 (ab179800, 1:1000; Abcam, Shanghai, China), iNOS (ab178945, 1:1000; Abcam), IL-6 (ab290735, 1:1000; Abcam), IL-1β (ab283818, 1:1000; Abcam), TNF-α (ab183218, 1:1000; Abcam), MCP-1 (ab315478, 1:1000; Abcam), β-actin (ab6276, 1:5000; Abcam), Bcl-2 (ab182858, 1:2000; Abcam), Bax (ab32503, 1:2000; Abcam), cleaved caspase-3 (ab214430, 1:5000; Abcam), phosphorylated IκBα (ab92700, 1:1000; Abcam), IκBα (ab32518, 1:2000; Abcam), phosphorylated p65 (ab76302, 1:1000; Abcam), and p65 (ab32536, 1:2000; Abcam) at 4°C. Subsequently, the membranes were washed three times using Tris Buffered Saline with Tween 20 (TBST; Sigma-Aldrich) and incubated with HRP-conjugated secondary antibodies for 2h at room temperature. After being washed three times with TBST, the protein bands were developed using an enhanced chemiluminescence reagent (Yeasen, Shanghai, China), and the intensity was quantified by ImageJ software (National Institutes of Health, Bethesda, Maryland, USA).

TUNEL immunofluorescence staining

A TUNEL staining kit (Beyotime) was used to assess apoptosis of kidney tissues. Briefly, kidney tissues were fixed in 10% neutral buffered formalin, embedded in paraffin, sectioned into 4-μm slices, and stained with the TUNEL kit. The nuclei were labeled with 4',6-diamidino-2-phenylindole (Sigma-Aldrich) at a dilution of 1:500. Positive staining with nuclear DNA fragmentation was detected by a fluorescence microscope (Olympus, Tokyo, Japan). Each section was randomly selected for ten representative fields, and TUNEL-positive cells (%) were quantified, by two blinded observers using ImageJ software, as the percentage of total renal cells.

Statistical analysis

Statistics were analyzed using GraphPad Prism 8 (GraphPad Software, San Diego, CA, USA). Data were described as the mean ± standard deviation. The significance between two groups was analyzed using the Student's *t*-test. Comparisons among multiple groups were analyzed by one-way analysis of variance followed

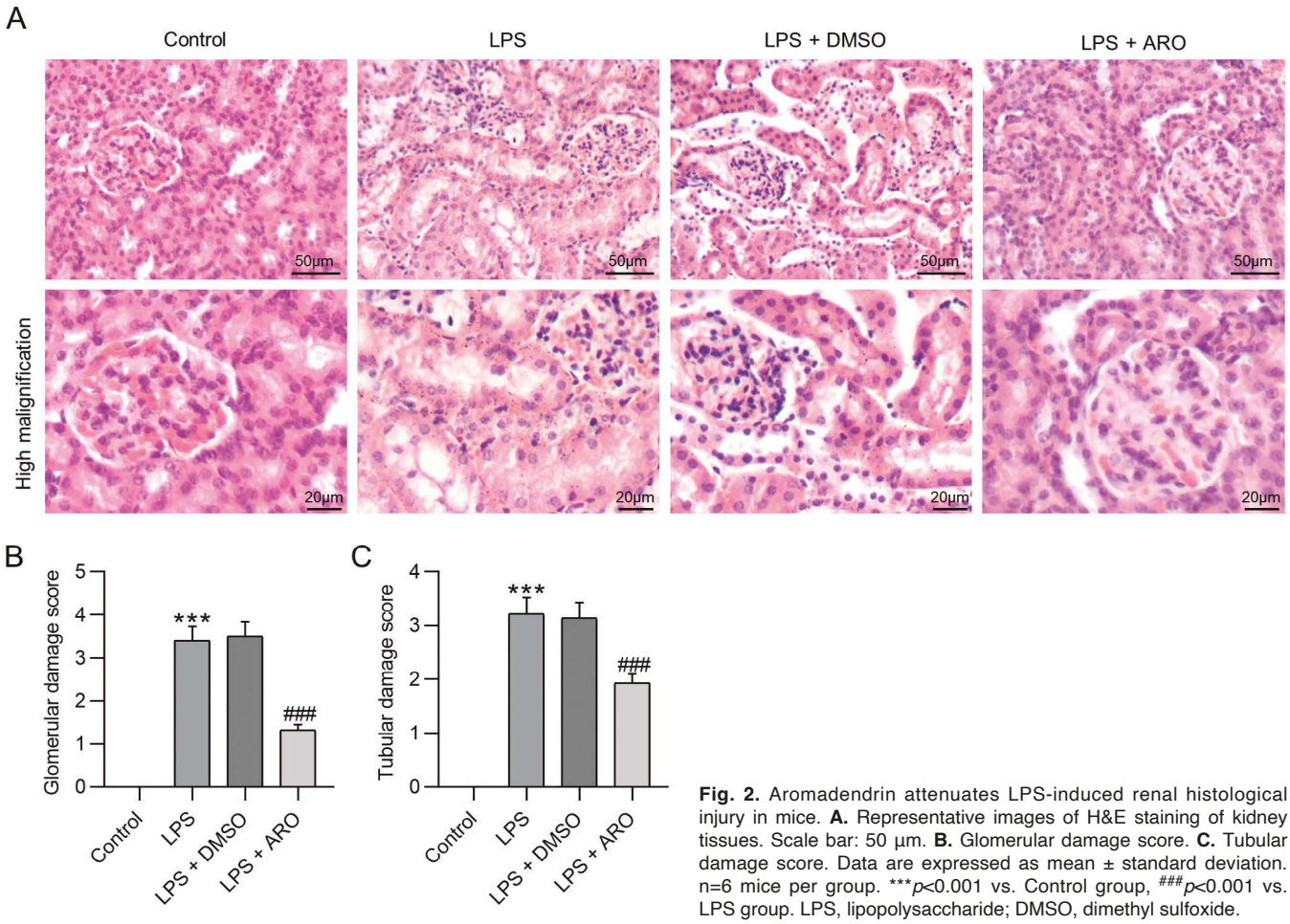

Fig. 2. Aromadendrin attenuates LPS-induced renal histological injury in mice. **A.** Representative images of H&E staining of kidney tissues. Scale bar: 50 μm. **B.** Glomerular damage score. **C.** Tubular damage score. Data are expressed as mean ± standard deviation. n=6 mice per group. ***$p<0.001$ vs. Control group, ###$p<0.001$ vs. LPS group. LPS, lipopolysaccharide; DMSO, dimethyl sulfoxide.

by Tukey's *post hoc* analysis. $p<0.05$ was considered statistically significant.

Results

Aromadendrin alleviates LPS-induced renal dysfunctions in mice

To evaluate aromadendrin toxicity in normal mice, serum levels of LDH were measured. The results revealed that serum biochemistry analysis of LDH showed no significant changes at 12, 24, or 48h after aromadendrin treatment in normal mice (Fig. 1A). Then, as shown by the data, LPS treatment led to significant increases in the serum levels of LDH at 12, 24, or 48h, whereas the increased levels of LDH were reduced by aromadendrin (Fig. 1B). Moreover, the serum levels of BUN and creatinine markedly increased in LPS-treated mice compared with those in the control group, whereas these LPS-induced increases were abolished by aromadendrin treatment (Fig. 1C,D). Notably, the LPS-induced renal dysfunctions were most severe at 24h; thus, we used kidney samples collected from mice at 24h after LPS challenge.

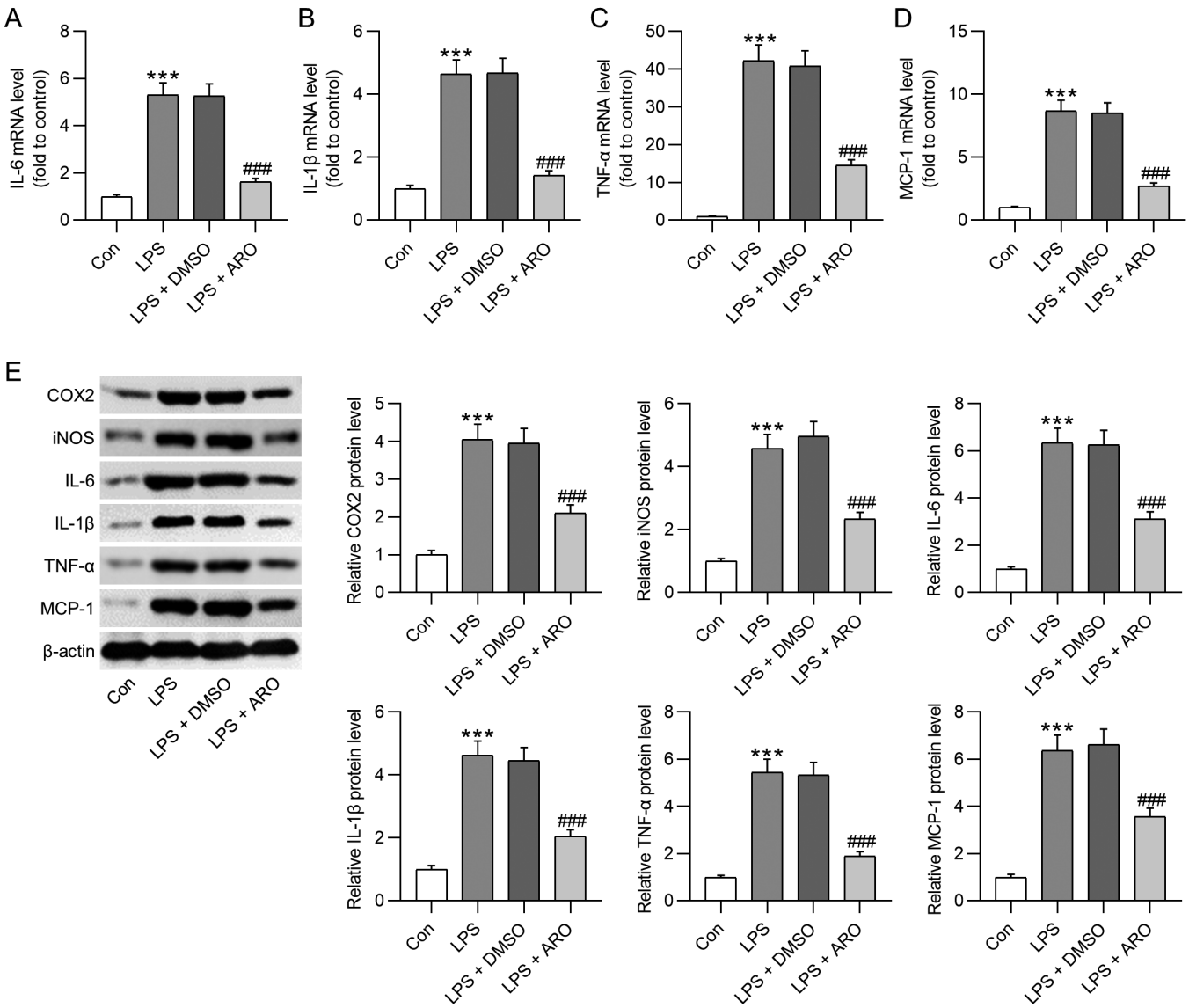

Fig. 3. Aromadendrin suppresses the LPS-induced inflammatory response in mice. **A-D.** The mRNA levels of IL-6, IL-1β, TNF-α, and MCP-1 were measured by RT-qPCR. **E.** The protein levels of COX-2, iNOS, IL-6, IL-1β, TNF-α, and MCP-1 were evaluated by western blotting. Data are expressed as mean ± standard deviation. n=4 mice per group. ***$p<0.001$ vs. Control group, ###$p<0.001$ vs. LPS group. LPS, lipopolysaccharide; IL-6, interleukin-6; IL-1β, interleukin-1β; TNF-α, tumor necrosis factor-alpha; MCP-1, monocyte chemoattractant protein-1; COX-2, cyclooxygenase (COX)-2; iNOS, inducible nitric oxide synthase.

Aromadendrin attenuates the LPS-induced renal histological injury in mice

Renal histopathological analysis was performed to evaluate kidney injury. The results of H&E staining showed that the renal structure in the control group was intact with no obvious signs of pathological kidney damage. However, the kidneys of LPS-treated mice showed significant glomerular damage (glomerular congestion and atrophy, mesangial matrix expansion, and mesangial cell proliferation) and tubular damage (swelling, necrosis, and vacuolar degeneration of renal tubular epithelial cells, renal tubular lumen expansion, and inflammatory cell infiltration). Administration of aromadendrin greatly improved these pathological changes (Fig. 2A). Then, the glomerular and tubular damages were scored semi-quantitatively. We found that, compared with the control group, the renal glomerular and tubular damage scores significantly increased in the LPS group. Aromadendrin treatment effectively reversed the effect of LPS on increasing glomerular and tubular damage scores (Fig. 2B,C). These results demonstrate that aromadendrin alleviates LPS-induced renal dysfunctions in mice.

Aromadendrin suppresses LPS-induced inflammation

Then, we detected the expression of pro-inflammatory mediators in kidney tissues. As revealed by RT-qPCR, IL-6, IL-1β, TNF-α, and MCP-1 mRNA levels were remarkably elevated by LPS, whereas administration of aromadendrin notably reduced their

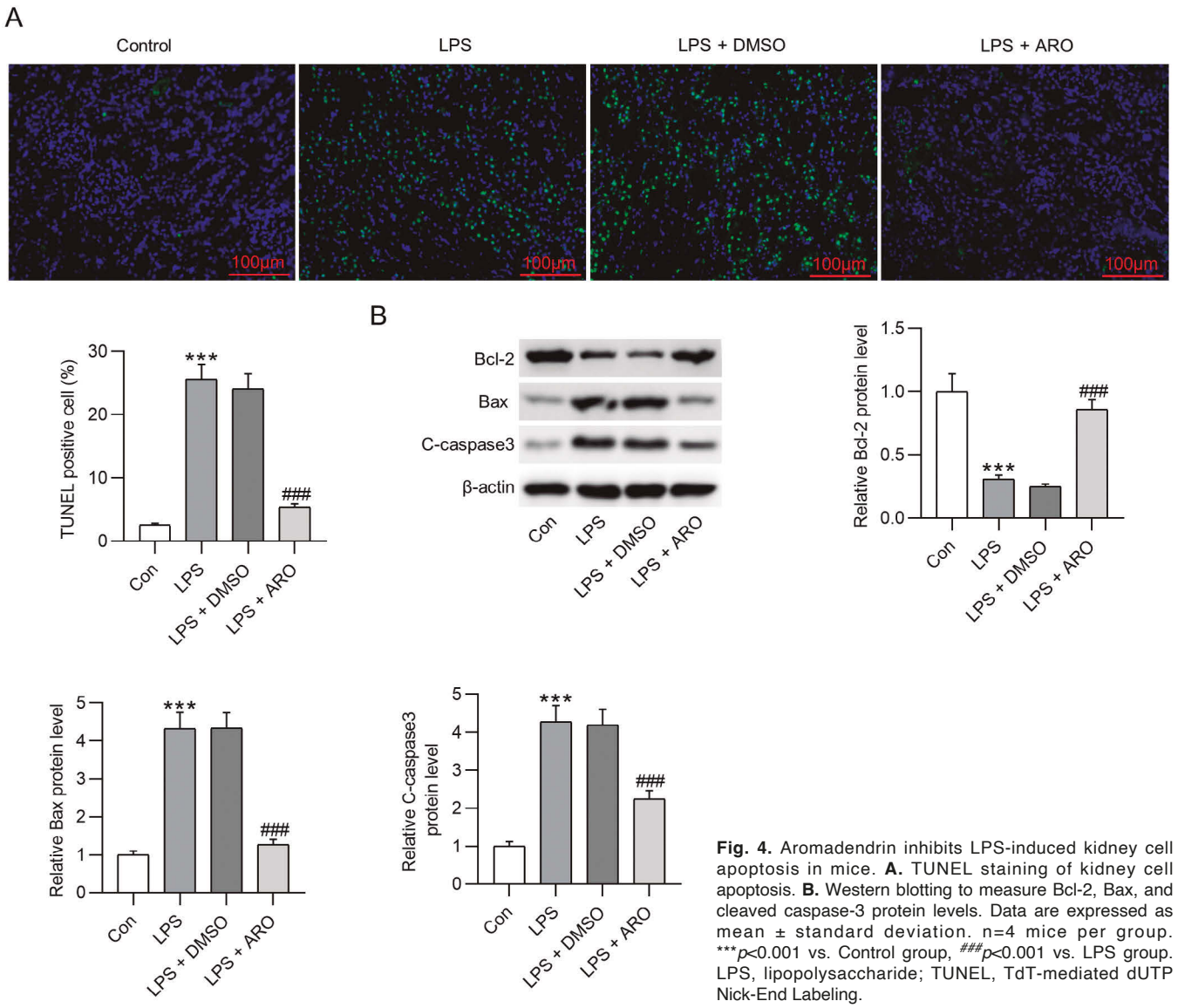

Fig. 4. Aromadendrin inhibits LPS-induced kidney cell apoptosis in mice. **A.** TUNEL staining of kidney cell apoptosis. **B.** Western blotting to measure Bcl-2, Bax, and cleaved caspase-3 protein levels. Data are expressed as mean ± standard deviation. n=4 mice per group. ***p<0.001 vs. Control group, ###p<0.001 vs. LPS group. LPS, lipopolysaccharide; TUNEL, TdT-mediated dUTP Nick-End Labeling.

mRNA levels (Fig. 3A-D). Consistently, the LPS-induced significant increase in protein levels of COX-2, iNOS, TNF-α, IL-1β, IL-6, and MCP-1 was effectively attenuated by aromadendrin treatment (Fig. 3E).

Aromadendrin inhibits LPS-induced tubular cell apoptosis in mice

Next, we detected the effect of aromadendrin on tubular cell apoptosis. As revealed by TUNEL, aromadendrin abolished the LPS-induced significant increase in the number of TUNEL-positive cells (Fig. 4A). Accordingly, LPS increased cleaved caspase-3 and Bax protein levels while decreasing Bcl-2 protein levels; aromadendrin reversed the effect of LPS on decreasing Bcl-2 protein levels and increasing Bax and cleaved caspase-3 protein levels (Fig. 4B).

Aromadendrin blocks the activation of NF-κB and MAPK pathways in LPS-induced AKI mice

Finally, we conducted western blotting to identify the anti-inflammatory and anti-apoptotic mechanisms of aromadendrin. We found that the phosphorylation levels of IκBα, p65, p38, ERK1/2, and JNK significantly increased with LPS, which were suppressed by aromadendrin (Fig. 5A,B). These results show that aromadendrin inactivates the NF-κB and MAPK pathways in LPS-induced AKI mice.

Discussion

Despite current efforts, the incidence and mortality of AKI remain high; thus, it is imperative to elucidate the underlying mechanisms of AKI and explore practical strategies for this disease. The dysregulated inflammatory response and cellular apoptosis in kidneys are critical players in the pathogenesis of AKI (Yang et al., 2019, 2021; Zhu et al., 2020). Aromadendrin has pharmacological actions such as anti-inflammation, antioxidation, and anti-apoptosis (Lee et al., 2009, 2013, 2021). Therefore, we investigated the roles and mechanisms of aromadendrin in AKI. Oral administration of aromadendrin protected against LPS-

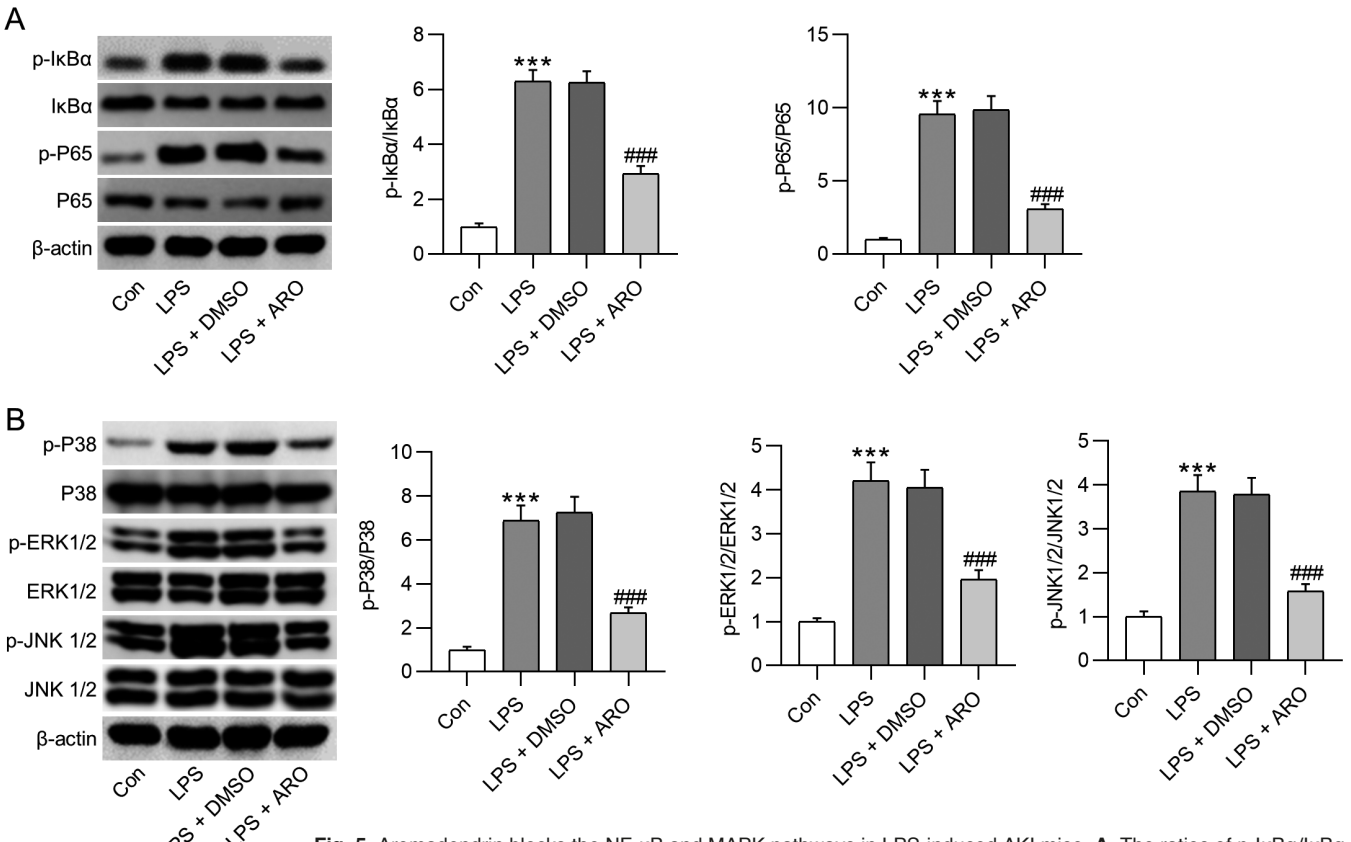

Fig. 5. Aromadendrin blocks the NF-κB and MAPK pathways in LPS-induced AKI mice. **A.** The ratios of p-IκBα/IκBα and p-p65/p65 were measured by western blotting. **B.** The ratios of p-p38/p38, p-ERK1/2/ERK1/2, and p-JNK/JNK were estimated by western blotting. Data are expressed as mean ± standard deviation. n=4 mice per group. ***p<0.001 vs. Control group, ###p<0.001 vs. LPS group. LPS, lipopolysaccharide; MAPK, mitogen-activated protein kinase; ERK, extracellular signal-regulated kinase; JNK, c-Jun N-terminal kinase; NF-κB, nuclear factor kappa B.

induced AKI via inactivation of the NF-κB and MAPK pathways as indicated by the following findings: a) aromadendrin attenuated the LPS-induced increases in LDH, BUN, and creatinine activities in serum; b) aromadendrin relieved LPS-induced renal histological dysfunctions; c) aromadendrin suppressed LPS-induced excessive inflammation and cellular apoptosis; d) aromadendrin reduced LPS-induced increases in the phosphorylation levels of IκBα, p65, p38, ERK1/2, and JNK.

As BUN and creatinine are recognized as two primary indicators of kidney dysfunction (Yue et al., 2022), we evaluated their activities in serum and found that LPS increased BUN and creatinine serum concentrations. Additionally, glomerular injury represents early manifestations of kidney injury and could indicate the risk of its development (Song et al., 2022). We used H&E staining to examine histological changes after LPS treatment and found the LPS-induced AKI was primarily attributed to glomerular lesions and inflammatory cell infiltration. Moreover, LPS can increase TNF-α, IL-1β, IL-6, MCP-1, iNOS, and COX-2 levels (Rousta et al., 2018; Qu et al., 2020). Inflammatory infiltration can induce kidney apoptosis and AKI (Rousta et al., 2018). Previous studies suggested that inhibition of Bcl-2 and activation of caspase-3 and Bax are recognized as predominant mechanisms responsible for renal tubular cell apoptosis (Kim et al., 2020; Li et al., 2021). In the current study, we found that LPS induced significant increases in COX-2, iNOS, IL-6, TNF-α, IL-1β, MCP-1, Bax, and cleaved caspase-3 levels while decreasing Bcl-2 expression. Simultaneously, LPS remarkably increased the number of TUNEL-positive cells. Collectively, LPS caused AKI as indicated by elevated BUN and creatinine levels, glomerular disorders, excessive inflammation, and cellular apoptosis. Flavonoids have been shown to have protective effects against LPS-induced AKI. For example, pectolinarigenin inhibits the Jak2/Stat3 pathway and mitochondria dysfunction to alleviate LPS-induced AKI (Tan et al., 2023). Alpinetin activates Nrf2 and inhibits TLR4 expression to protect LPS-induced AKI (Huang et al., 2015). Licochalcone A inhibits NF-κB activation to attenuate LPS-induced AKI (Hu and Liu, 2016). Aromadendrin, a bioactive flavonoid isolated from *Pinus sibirica*, *Afzelia bella*, and *Chioanathus retusus*, has anti-inflammatory and antiapoptotic properties. Aromadendrin can mitigate methamphetamine-induced apoptosis in methamphetamine-challenged SH-SY5Y cells (Lee et al., 2021). Additionally, aromadendrin can suppress the LPS-induced excessive production of proinflammatory mediators by inactivating the NF-κB and JNK pathways (Lee et al., 2013). Herein, we found that aromadendrin attenuated the LPS-induced BUN and creatinine elevation, renal histological defects, excessive inflammation, and cellular apoptosis.

LPS is a ligand of TLR4, activation of which sensitizes the NF-κB and MAPK pathways and thereby amplifies excessive inflammation (He et al., 2013). Reportedly, aromadendrin can inhibit the nuclear translocation of NF-κB and phosphorylation of JNK in LPS-stimulated RAW 264.7 macrophages (Lee et al., 2013). Additionally, aromadendrin has been found to alleviate allergic asthma by inhibiting the activation of NF-κB in experimental models (Park et al., 2023). In the current study, we found that aromadendrin inactivated the NF-κB and MAPK pathways in LPS-induced AKI mice.

However, this study has some limitations. First, the conclusions in this study were obtained from preclinical animal experiments, which can not be transferred to human samples directly. Second, the nuclear translocation of p65 has not been confirmed by immunofluorescence staining. Third, we only studied the effect of aromadendrin on the NF-κB and MAPK pathways and LPS-induced AKI. Further studies are required to determine the mechanisms and relationship between these pathways and LPS-induced AKI.

In conclusion, this study revealed that aromadendrin administration attenuated LPS-induced excessive inflammation and cell apoptosis in kidneys via inactivation of the NF-κB and MAPK pathways. Thus, this study provides a theoretical basis for the clinical application of aromadendrin in treating AKI.

Acknowledgements. The authors appreciate the help of Shenzhen Bao'an Authentic Tcm Therapy Hospital.

Conflict of interest. None.

Ethics approval. All experimental protocols and procedures complied with the National Institutes of Health Guide for the Care and Use of Laboratory Animals and were approved by the Ethics Review Committee of Wuhan Myhalic Biotechnology Co., Ltd (HLK-202206126).

Funding. This work was supported by the 2021 Shenzhen Baoan District Basic Research (Medical and Health) Project (Shenzhen Baoan District Science and Technology Innovation Bureau) (No. 2021JD164).

References

Ban K.Y., Nam G.Y., Kim D., Oh Y.S. and Jun H.S. (2022). Prevention of LPS-induced acute kidney injury in mice by bavachin and its potential mechanisms. Antioxidants 11, 2096.

Basile D.P., Anderson M.D. and Sutton T.A. (2012). Pathophysiology of acute kidney injury. Compr. Physiol. 2, 1303-1353

Chen Y., Jin S., Teng X., Hu Z., Zhang Z., Qiu X., Tian D. and Wu Y. (2018). Hydrogen sulfide attenuates LPS-induced acute kidney injury by inhibiting inflammation and oxidative stress. Oxid. Med. Cell Longev. 2018, 6717212.

Coca S.G., Yusuf B., Shlipak M.G., Garg A.X. and Parikh C.R. (2009). Long-term risk of mortality and other adverse outcomes after acute kidney injury: a systematic review and meta-analysis. Am. J. Kidney Dis. 53, 961-973

Dellepiane S., Marengo M. and Cantaluppi V. (2016). Detrimental cross-talk between sepsis and acute kidney injury: new pathogenic mechanisms, early biomarkers and targeted therapies. Crit. Care 20, 61.

Ding Q., Wang Y., Zhang A.L., Xu T., Zhou D.D., Li X.F., Yang J.F.,

Zhang L. and Wang X. (2018). ZEB2 attenuates LPS-induced inflammation by the NF-κB pathway in HK-2 cells. Inflammation 41, 722-731.

Gong Q., Ma J., Kang H., Pan X. and You Y. (2022). Fractalkine deficiency attenuates LPS-induced acute kidney injury and podocyte apoptosis by targeting the PI3K/Akt signal pathway. Clin. Exp. Nephrol. 26, 741-749.

Goyal A., Daneshpajouhnejad P., Hashmi M.F. and Bashir K. (2023). Acute kidney injury. StatPearls Publishing LLC.

Guzzi F., Cirillo L., Roperto R.M., Romagnani P. and Lazzeri E. (2019). Molecular mechanisms of the acute kidney injury to chronic kidney disease transition: An updated view. Int. J. Mol. Sci. 20, 4941.

He W., Qu T., Yu Q., Wang Z., Lv H., Zhang J., Zhao X. and Wang P. (2013). LPS induces IL-8 expression through TLR4, MyD88, NF-kappaB and MAPK pathways in human dental pulp stem cells. Int. Endod. J. 46, 128-136.

Hu J. and Liu J. (2016). Licochalcone A attenuates Lipopolysaccharide-Induced acute kidney injury by inhibiting NF-κB activation. Inflammation 39, 569-574.

Huang Y., Zhou L.S., Yan L., Ren J., Zhou D.X. and Li S.S. (2015). Alpinetin inhibits lipopolysaccharide-induced acute kidney injury in mice. Int. Immunopharmacol. 28, 1003-1008.

Ichai C., Vinsonneau C., Souweine B., Armando F., Canet E., Clec'h C., Constantin J.M., Darmon M., Duranteau J., Gaillot T., Garnier A., Jacob L., Joannes-Boyau O., Juillard L., Journois D., Lautrette A., Muller L., Legrand M., Lerolle N., Rimmelé T., Rondeau E., Tamion F., Walrave Y., Velly L., Société française d'anesthésie et de réanimation (Sfar), Société de réanimation de langue française (SRLF), Groupe francophone de réanimation et urgences pédiatriques (GFRUP) and Société française de néphrologie (SFN) (2016). Acute kidney injury in the perioperative period and in intensive care units (excluding renal replacement therapies). Ann. Intensive Care 6, 48.

Kim I.Y., Park Y.K., Song S.H., Seong E.Y., Lee D.W., Bae SS. and Lee S.B. (2020). Akt1 is involved in tubular apoptosis and inflammatory response during renal ischemia-reperfusion injury. Mol. Biol. Rep. 47, 9511-9520.

Kökény G., Fang L., Révész C., Mózes M.M., Vörös P., Szénási G. and Rosivall L. (2017). The effect of combined treatment with the (Pro)Renin receptor blocker HRP and quinapril in Type 1 diabetic rats. Kidney Blood Press. Res. 42, 109-122.

Lee H.S. and Jeong G.S. (2020). Aromadendrin inhibits T cell activation via regulation of calcium influx and NFAT activity. Molecules 25, 4590.

Lee Y.J., Kim S., Lee S.J., Ham I. and Whang W.K. (2009). Antioxidant activities of new flavonoids from Cudrania tricuspidata root bark. Arch. Pharm. Res. 32, 195-200.

Lee J.W., Kim N.H., Kim J.Y., Park J.H., Shin S.Y., Kwon Y.S., Lee H.J., Kim S.S. and Chun W. (2013). Aromadendrin inhibits Lipopolysaccharide-Induced nuclear translocation of NF-κB and phosphorylation of JNK in RAW 264.7 macrophage cells. Biomol. Ther. (Seoul) 21, 216-221.

Lee H.S., Kim E.N. and Jeong G.S. (2021). Aromadendrin protects neuronal cells from Methamphetamine-Induced neurotoxicity by regulating endoplasmic reticulum stress and PI3K/Akt/mTOR signaling pathway. Int. J. Mol. Sci. 22, 2274.

Li J., Zhang Z., Wang L., Jiang L., Qin Z., Zhao Y. and Su B. (2021). Maresin 1 attenuates Lipopolysaccharide-Induced acute kidney injury via inhibiting NOX4/ROS/NF-κB pathway. Front. Pharmacol. 12, 782660.

Liang H., Liu H.Z., Wang H.B., Zhong J.Y., Yang C.X. and Zhang B. (2017). Dexmedetomidine protects against cisplatin-induced acute kidney injury in mice through regulating apoptosis and inflammation. Inflamm. Res. 66, 399-411.

Livak K.J. and Schmittgen T.D. (2001). Analysis of relative gene expression data using real-time quantitative PCR and the 2(-Delta Delta C(T)) method. Methods 25, 402-408.

Ma Y., Liu J., Liu H., Han X., Sun L. and Xu H. (2022). Podocyte protection by Angptl3 knockout via inhibiting ROS/GRP78 pathway in LPS-induced acute kidney injury. Int. Immunopharmacol. 105, 108549.

Park J.M., Park J.W., Lee J., Kim S.H., Seo D.Y., Ahn K.S., Han S.B. and Lee J.W. (2023). Aromadendrin inhibits PMA-induced cytokine formation/NF-κB activation in A549 cells and ovalbumin-induced bronchial inflammation in mice. Heliyon 9, e22932.

Peerapornratana S., Manrique-Caballero C.L., Gómez H. and Kellum J.A. (2019). Acute kidney injury from sepsis: current concepts, epidemiology, pathophysiology, prevention and treatment. Kidney Int. 96, 1083-1099.

Qu Y., Sun Q., Song X., Jiang Y., Dong H., Zhao W. and Li C. (2020). Helix B surface peptide reduces sepsis-induced kidney injury via PI3K/Akt pathway. Nephrology 25, 527-534.

Reiser J. and Altintas M.M. (2016). Podocytes. F1000Res 5, F1000.

Rousta A.M., Mirahmadi S.M., Shahmohammadi A., Nourabadi D., Khajevand-Khazaei M.R., Baluchnejadmojarad T. and Roghani M. (2018). Protective effect of sesamin in lipopolysaccharide-induced mouse model of acute kidney injury via attenuation of oxidative stress, inflammation, and apoptosis. Immunopharmacol. Immunotoxicol. 40, 423-429.

Sever S. and Schiffer M. (2018). Actin dynamics at focal adhesions: a common endpoint and putative therapeutic target for proteinuric kidney diseases. Kidney Int. 93, 1298-1307.

Song W., Zhou X., Duan Q., Wang Q., Li Y., Li A., Zhou W., Sun L., Qiu L., Li R. and Li Y. (2022). Using random forest algorithm for glomerular and tubular injury diagnosis. Front. Med. 9, 911737.

Tan Z., Liu Q., Chen H., Zhang Z., Wang Q., Mu Y., Li Y., Hu T., Yang Y. and Yan X. (2023). Pectolinarigenin alleviated septic acute kidney injury via inhibiting Jak2/Stat3 signaling and mitochondria dysfunction. Biomed. Pharmacother. 159, 114286.

Tang Y., Luo H., Xiao Q., Li L., Zhong X., Zhang J., Wang F., Li G., Wang L. and Li Y. (2021). Isoliquiritigenin attenuates septic acute kidney injury by regulating ferritinophagy-mediated ferroptosis. Ren. Fail. 43, 1551-1560.

Van Amersfoort E.S., Van Berkel T.J. and Kuiper J. (2003). Receptors, mediators, and mechanisms involved in bacterial sepsis and septic shock. Clin. Microbiol. Rev. 16, 379-414.

Yang Q., Ren G.L., Wei B., Jin J., Huang X.R., Shao W., Li J., Meng X.M. and Lan H.Y. (2019). Conditional knockout of TGF-βRII /Smad2 signals protects against acute renal injury by alleviating cell necroptosis, apoptosis and inflammation. Theranostics 9, 8277-8293.

Yang Q., Zang H.M., Xing T., Zhang S.F., Li C., Zhang Y., Dong Y.H., Hu X.W., Yu J.T., Wen J.G., Jin J., Li J., Zhao R., Ma T.T. and Meng X.M. (2021). Gypenoside XLIX protects against acute kidney injury by suppressing IGFBP7/IGF1R-mediated programmed cell death and inflammation. Phytomedicine 85, 153541.

Yoo H., Ku S.K., Han M.S., Kim K.M. and Bae J.S. (2014). Anti-septic effects of fisetin *in vitro* and *in vivo*. Inflammation 37, 1560-

1574.

Yoon S.Y., Kim J.S., Jeong K.H. and Kim S.K. (2022). Acute kidney injury: Biomarker-guided diagnosis and management. Medicina 58, 340.

Yue S., Li S., Huang X., Liu J., Hou X., Wang Y. and Wu J. (2022). Construction and validation of a risk prediction model for acute kidney injury in patients suffering from septic shock. Dis. Markers 2022, 9367873.

Zhang X., Hung T.M., Phuong P.T., Ngoc T.M., Min B.S., Song K.S., Seong Y.H. and Bae K (2006). Anti-inflammatory activity of flavonoids from Populus davidiana. Arch. Pharm. Res. 29, 1102-1108.

Zhang W.Y., Lee J.J., Kim I.S., Kim Y. and Myung C.S. (2011). Stimulation of glucose uptake and improvement of insulin resistance by aromadendrin. Pharmacology 88, 266-274.

Zhang B., Zeng M., Li B., Kan Y., Wang S., Cao B., Huang Y., Zheng X. and Feng W. (2021). Arbutin attenuates LPS-induced acute kidney injury by inhibiting inflammation and apoptosis via the PI3K/Akt/Nrf2 pathway. Phytomedicine 82, 153466.

Zhang F., Luo X., Wang Y., Ma L. and Sun D. (2023). LncRNA PMS2L2 is downregulated in sepsis-induce acute kidney injury and inhibits LPS-induced apoptosis of podocytes. Kidney Blood Press. Res. 48, 515-521.

Zhu H., Wang X., Wang X., Liu B., Yuan Y. and Zuo X. (2020). Curcumin attenuates inflammation and cell apoptosis through regulating NF-κB and JAK2/STAT3 signaling pathway against acute kidney injury. Cell Cycle 19, 1941-1951.

Zhuo Y., Li D., Cui L., Li C., Zhang S., Zhang Q., Zhang L., Wang X. and Yang L. (2019). Treatment with 3,4-dihydroxyphenylethyl alcohol glycoside ameliorates sepsis-induced ALI in mice by reducing inflammation and regulating M1 polarization. Biomed. Pharmacother. 116, 109012.

Accepted May 30, 2024